bioRxiv preprint doi: https://doi.org/10.1101/2021.04.08.439081; this version posted April 9, 2021. The copyright holder for this preprint (which was not certified by peer review) is the author/funder, who has granted bioRxiv a license to display the preprint in perpetuity. It is made available under aCC-BY-NC-ND 4.0 International license.

Modern *Acinetobacter baumannii* clinical isolates replicate inside spacious vacuoles and egress from macrophages.

Gabriela Sycz[1¶], Gisela Di Venanzio[1¶], Mariana G. Sartorio[1], Le Nguyen- Hung[1], Nichollas E. Scott[2], Wandy L. Beatty[1], Mario F. Feldman[1*].

[1] Department of Molecular Microbiology, Washington University School of Medicine, Saint Louis, Missouri, United States of America.

[2] Department of Microbiology and Immunology, The Peter Doherty Institute for Infection and Immunity, University of Melbourne, Parkville, Victoria, Australia.

*Corresponding author:

E-mail: mariofeldman@wustl.edu (MFF)

¶ These authors contributed equally to this work.

bioRxiv preprint doi: https://doi.org/10.1101/2021.04.08.439081; this version posted April 9, 2021. The copyright holder for this preprint (which was not certified by peer review) is the author/funder, who has granted bioRxiv a license to display the preprint in perpetuity. It is made available under aCC-BY-NC-ND 4.0 International license.

Abstract

Multidrug-resistant *Acinetobacter baumannii* infections are increasing at alarming rates. Therefore, novel antibiotic-sparing treatments to combat these *A. baumannii* infections are urgently needed. The development of these interventions would benefit from a better understanding of this bacterium's pathobiology, which remains poorly understood. *A. baumannii* is regarded as an extracellular opportunistic pathogen. However, research on *Acinetobacter* has largely focused on common lab strains, such as ATCC 19606, that have been isolated several decades ago. These strains exhibit reduced virulence when compared to recently isolated clinical strains. In this work, we demonstrate that, unlike ATCC 19606, several modern *A. baumannii* clinical isolates, including the recent clinical urinary isolate UPAB1, persist and replicate inside macrophages within spacious vacuoles. We show that intracellular replication of UPAB1 is dependent on a functional type I secretion system (T1SS) and pAB5, a large conjugative plasmid that controls the expression of several chromosomally-encoded genes. Finally, we show that UPAB1 escapes from the infected macrophages by a lytic process. To our knowledge, this is the first report of intracellular growth and replication of *A. baumannii*. We suggest that intracellular replication within macrophages may contribute to evasion of the immune response, dissemination, and antibiotic tolerance of *A. baumannii*.

bioRxiv preprint doi: https://doi.org/10.1101/2021.04.08.439081; this version posted April 9, 2021. The copyright holder for this preprint (which was not certified by peer review) is the author/funder, who has granted bioRxiv a license to display the preprint in perpetuity. It is made available under aCC-BY-NC-ND 4.0 International license.

Introduction

Infections caused by the bacterial pathogen *Acinetobacter baumannii* are a global public health risk since multidrug resistance (MDR) increasingly limits effective therapeutic interventions [1,2]. The emerging success of this pathogen has led the World Health Organization (WHO) and the CDC to categorize carbapenem-resistant *A. baumannii* as a top priority for the research and development of new antibiotics [3,4]. However, compared to other opportunistic pathogens, our knowledge about the pathobiology of *Acinetobacter* is rather limited.

Research on *Acinetobacter* has largely focused on common lab strains that have been "lab-domesticated" over ~50 years. These non-MDR strains exhibit reduced virulence when compared to recently isolated clinical strains, indicating that classical lab strains lack virulence factors expressed by current-day strains [5,6]. Consequently, little is known about the virulence factors and molecular pathways governing modern *A. baumannii* infections. Although *A. baumannii* is best known as a respiratory pathogen, infection of various anatomical sites is also common. For example, urinary tract infections (UTI) account for about ~20% of *A. baumannii* infections worldwide). We recently developed a murine model of *A. baumannii* catheter-associated urinary tract infection (CAUTI)[5]. Using this model, we compared the behavior of two urinary *A. baumannii* isolates, ATCC19606 (19606) and UPAB1. 19606 is a urinary isolate obtained in 1967, and it has been routinely used to study *A. baumannii* virulence. UPAB1 is a modern MDR UTI isolate, collected from a female patient in 2016. We demonstrated that, unlike 19606, which was rapidly cleared from infected mice, UPAB1 was able to establish early implant and bladder colonization[5]. These findings suggested that "old" and "new" strains have a different repertoire of virulence or fitness factors, which can influence the outcome of the infection. Interestingly, UPAB1 carries a large conjugative plasmid (LCP), pAB5, which controls the expression of multiple virulence factors. Remarkably, pAB5 impacts the pathogenicity of UPAB1 in the CAUTI and acute pneumonia murine models[5].

A few reports have suggested that classical *A. baumannii* strains are able to persist within epithelial cells. It has been suggested that the intracellular bacterial cells are contained by membrane-bound vacuoles, likely of autophagic origin, and subsequently eliminated by the intracellular vesicular pathway[7–10]. In this work, we demonstrate that unlike 19606, several modern *A. baumannii* clinical isolates, including UPAB1, persist and, remarkably, replicate inside macrophages within spacious vacuoles containing up to more than 30 bacteria. We show that intracellular replication of UPAB1 is dependent on pAB5 and a functional Type I Secretion System (T1SS). Finally, we also show that UPAB1 escapes from the infected macrophages by a

bioRxiv preprint doi: https://doi.org/10.1101/2021.04.08.439081; this version posted April 9, 2021. The copyright holder for this preprint (which was not certified by peer review) is the author/funder, who has granted bioRxiv a license to display the preprint in perpetuity. It is made available under aCC-BY-NC-ND 4.0 International license.

lytic process. To the best of our knowledge, this is the first report of intracellular growth and replication of *A. baumannii*.

Results

UPAB1 but not 19606 replicates in spacious intracellular vacuoles within macrophages

Macrophages play an important role in early host defense against *A. baumannii*. Indeed, depletion of macrophages enhances sepsis and severity of *A. baumannii* infection [11]. Macrophages can efficiently control the replication and kill the most common lab strains, such as ATCC 17978 and 19606, which have been isolated more than half a century ago. However, whether modern clinical isolates can be efficiently phagocytosed and eliminated by macrophages has not been investigated. To this end, we tested the ability of the modern *A. baumannii* isolate UPAB1 to resist macrophage-killing. J774A.1 macrophages were infected at an MOI of 10 and visualized by TEM. We found that UPAB1-infected J774A.1 macrophages possessed spacious vacuoles containing up to 15 bacteria per vacuole (Fig. 1A). Hereafter, we refer to these structures as *A. baumannii*-Containing Vacuoles (ACVs). A double membrane was visible in about half of the ACVs, which is compatible with an autophagic origin (Fig. 1B). This result is in agreement with previous reports showing that *A. baumannii* lab strains are contained within autophagic ACVs in epithelial cells [12]. CFU enumeration of intracellular bacteria (Fig. 2A) showed that UPAB1 can replicate intracellularly between 2 to 6 h p.i. In contrast, the lab strain 19606 was efficiently eliminated and no intracellular replication was detected (Fig. 2A). Visualization of intracellular bacteria by confocal microscopy demonstrated the presence of small ACVs at 2.5 h p.i and some large ACVs, containing more than 20 bacteria per vacuole, at 5 and 7 h p. i. (Fig. 2B). Indeed, the number of bacteria per ACV increased with time (Fig. 2B, C and S1). We were able to detect vacuoles with up to 30 to 40 intracellular UPAB1 between 5 to 7 h p. i. Almost no intracellular bacteria were observed in macrophages infected with 19606 at similar time points (Fig. 2B, right panel). Together, these experiments demonstrate that UPAB1 is able to infect, persist and replicate intracellularly in J774A.1 macrophages. Large ACVs were also observed in human THP-1 cells (Fig 3 left panel) and, remarkably, in murine bone-marrow-derived macrophages (BMDM) (Fig 3 right panel and S1), indicating that intracellular replication of UPAB1 is a phenomenon that occurs in multiple host cell lines and does not depend on a permissive host cell. For the remainder of the study, we will employ J774A.1 macrophages as host cells.

Several MDR clinical isolates replicate inside macrophages

bioRxiv preprint doi: https://doi.org/10.1101/2021.04.08.439081; this version posted April 9, 2021. The copyright holder for this preprint (which was not certified by peer review) is the author/funder, who has granted bioRxiv a license to display the preprint in perpetuity. It is made available under aCC-BY-NC-ND 4.0 International license.

Lab-domesticated strains generally exhibit reduced virulence in animal models when compared to recently isolated clinical strains, a possible indication that classical lab strains lack virulence factors expressed by current-day strains[13]. We next tested if other recent MDR clinical isolates were able to replicate in macrophages (Fig. 4). Although at different rates, these strains also replicated in J774A.1 macrophages (Fig. 4A). Large ACV were observed for the two additional strains tested (Fig. 4B), demonstrating that intracellular replication is not a unique feature of UPAB1.

UPAB1 ACV are LC3-negative

Autophagy is a well-established intracellular mechanism by which the eukaryotic cells eliminate unwanted components, including invading pathogens[14]. However, some intracellular pathogens are able to grow in vacuoles with autophagic features, like *Serratia marcescens and Coxiella burnetii* [15,16]. Several studies employing non-replicative *A. baumannii* lab strains have proposed that upon infection, the autophagic pathway is activated in host cells, leading to an accumulation of LC3-positive vacuoles[8]. Although many alternative molecular pathways have been described in the autophagic process, one common characteristic of the autophagic vacuoles is a double membrane and the presence of the protein LC3 in both membranes[17]. As some of the UPAB1-containing vacuoles exhibited a double membrane, we investigated if these vacuoles contained LC3 (Fig. S2). Uninfected macrophages showed a smooth cytoplasmic distribution of LC3, characteristic of non-autophagic processes (Fig. S2A). *Serratia marcescens* RM66262 vacuoles were LC3-positive at 2 h p.i. (Fig. S2B), as previously described[15]. However, no LC3-positive vacuoles (Fig. S2C) were visualized in cells infected with UPAB1 at all the observed time points (1 to 5 h p.i.), suggesting that the replicative ACV follow a different intracellular pathway than the ACV previously described for non-replicative strains.

UPAB1 escapes the macrophages by a lytic process

Our results show that intracellular CFUs of UPAB1 in J774A.1 peak at 4-6 h pi, and then decrease at later time points (Fig. 2A). This decline may be the result of bacterial death inside the vacuoles. Alternatively, the reduction in the CFUs of intracellular bacteria could reflect the egress of bacteria from the infected macrophage to the extracellular media. To investigate these hypotheses, we carried out a modified antibiotic protection assay. In this assay, antibiotics were added 1 h p.i. to eliminate extracellular non-phagocytosed bacteria. At different time points, the antibiotic-containing medium was replaced by fresh cell culture medium without antibiotics. After

bioRxiv preprint doi: https://doi.org/10.1101/2021.04.08.439081; this version posted April 9, 2021. The copyright holder for this preprint (which was not certified by peer review) is the author/funder, who has granted bioRxiv a license to display the preprint in perpetuity. It is made available under aCC-BY-NC-ND 4.0 International license.

a 20-min incubation, the culture supernatants from each well were recovered and the number of released bacteria were quantified. The ratio of released bacteria in relation to the numbers of intracellular bacteria corresponding to each time interval is shown in Figure 5A. Our data suggests that intracellular UPAB1 cells egress from the macrophages. To confirm this result, we inspected the infected macrophages with UPAB1-GFP through live-video microscopy. We observed bacteria egressing the macrophages through a process that lysed the host cells (Fig 5B). Lactate dehydrogenase (LDH), a soluble cytosolic enzyme present in eukaryotic cells, is released into the culture medium upon damage to the plasma membrane[18]. The increase of LDH activity in culture supernatant is proportional to the number of damaged cells. Accordingly, we detected a significant increase in LDH activity in macrophages infected with UPAB1 compared to non-infected macrophages (Fig. 5C). Together, these results indicate that UPAB1 can survive and replicate inside macrophages and then escape from these cells through a lytic process. Although the mechanism for these processes will require further studies, it is tempting to speculate that UPAB1, like other bacteria that replicate and escape from the vacuole, manipulates the host cell through the activity of secreted proteins.

UPAB1 replication in macrophages relies on pAB5

LCPs are a family of large conjugative plasmids present in many *A. baumannii* strains[19]. In previous work, we showed that pAB5, the LCP carried by UPAB1 greatly impacts virulence, as its presence is required for the establishment of infection in a CAUTI model but detrimental for virulence in an acute respiratory murine model[20]. Thus, we investigated if the presence of pAB5 also impacts the ability of UPAB1 to replicate in macrophages. The strain cured of its plasmid (UPAB1p-) was unable to replicate in J774A.1 macrophages (Fig. 6A), and intracellular CFUs quickly decreased after phagocytosis, indicating that UPAB1p- is efficiently eliminated by macrophages. These results suggest that pAB5 is required for UPAB1 replication and persistence inside macrophages. We have previously shown that LCP controls the expression of the type VI secretion system (T6SS) [21]. We also found that pAB5 modulates the expression of other chromosomally-encoded factors. For example, pAB5 represses the synthesis of poly-N-acetyl-β-(1-6)-glucosamine (PNAG), a surface polysaccharide that plays an important role in biofilm formation *in vitro*, and reduces the expression of two chaperone-usher pili, CUP1 and CUP2, which are required for adhesion to fibrinogen and possibly other host receptors during infection[5]. Most bacteria that are able to survive and replicate inside macrophages secrete proteins via secretion systems, commonly T3SS, T4SS, T6SS, or T7SS[22]. These effectors allow the bacteria to manipulate host signaling and trafficking pathways to create a replicative

bioRxiv preprint doi: https://doi.org/10.1101/2021.04.08.439081; this version posted April 9, 2021. The copyright holder for this preprint (which was not certified by peer review) is the author/funder, who has granted bioRxiv a license to display the preprint in perpetuity. It is made available under aCC-BY-NC-ND 4.0 International license.

niche within the macrophage. *Acinetobacter* spp. do not encode T3SS or T4SS, but carry T1SS, T2SS and T6SSs[23]. However, the T6SS in *Acinetobacter* appears to be only involved in interbacterial competition, as many recent clinical isolates do not carry a functional T6SS[24]. Our previous proteomic and RNAseq experiments showed that pAB5 increases the expression of a T1SS-secreted agglutinin RTX toxin (D1G37_00080), and an adjacently-encoded protein, OmpA[5]. This observation prompted us to investigate a possible role for the T1SS in the intracellular replication of UPAB1.

T1SS is required for UPAB1 intracellular replication

The T1SS is a highly conserved secretion system employed by pathogenic Gram-negative bacteria. This secretion machinery is composed of an ATP-binding cassette transporter anchored in the inner membrane (HlyB), a periplasmic adaptor protein (HlyD) and a third component localized in the outer membrane (TolC). Together, these elements act to facilitate the secretion of unfolded effectors from the cytoplasm to the extracellular milieu[25]. UPAB1 encodes two T1SS clusters, which we named T1SSa and T1SSb (Fig. 6B). We generated ΔT1SSa, ΔT1SSb and ΔT1SSab mutant strains and analyzed their replication within macrophages. We found that all three T1SS deficient strains were unable to replicate inside J774A.1 macrophages (Fig 6C).

To identify putative T1SS-dependent effectors involved in survival and replication within macrophages, we employed a differential proteomics approach. A comparative secretome analysis between WT UPAB1 and the T1SSa and T1SSb mutant strains was performed. Table 1 lists the secreted proteins diminished in ΔT1SSa and ΔT1SSb compared to WT. We were able to identify multiple T1SS effector candidates. T1SS effectors BapA and RTX2, two common T1SS effectors, were repressed in ΔT1SSa. Neither of these proteins were repressed in ΔT1SSb, suggesting T1SSa is the preferred secretion system employed for the export of these two proteins. Our analysis also identified additional potential T1SS effectors, including proteases, phosphatases, glycosidases, and a putative invasin (table 1). In other bacteria, orthologs of invasin are required to induce bacterial entry and simultaneously to block the generation of reactive oxygen species (ROS) by host monocytes and macrophages[26]. Although the identification of the T1SS effectors directly involved in intracellular replication is beyond the scope of this work, our experiments demonstrate that T1SSs play a role in the process, and our MS analysis identified several interesting candidates that will be the subject of future studies.

bioRxiv preprint doi: https://doi.org/10.1101/2021.04.08.439081; this version posted April 9, 2021. The copyright holder for this preprint (which was not certified by peer review) is the author/funder, who has granted bioRxiv a license to display the preprint in perpetuity. It is made available under aCC-BY-NC-ND 4.0 International license.

Discussion

Although intracellular survival of *A. baumannii* inside vacuoles has been reported, the capacity of this bacterium to replicate intracellularly has not been documented. Here, we show that modern clinical isolates, such as UPAB1, can replicate inside spacious vacuoles within macrophages. Previous reports have shown that non-replicating *A. baumannii* can induce autophagy in epithelial cells and macrophages and indicated that autophagy is required for clearance of intracellular bacteria[7–10]. TEM predominantly exhibited double-membrane enclosed vacuoles, which is indicative of an autophagic origin for the ACV. However, we found that ACVs formed by UPAB1 are LC3-negative, suggesting that these replicative ACVs do not follow a canonical autophagy pathway. This is in agreement with findings from the Salcedo group, demonstrating that modern clinical isolates replicate within non-autophagic ACV in epithelial cells (personal communication). It remains to be determined whether these observations are the result of LC3 degradation induced by UPAB1 or an indication that UPAB1 evades the canonical autophagy pathway before LC3 is recruited to the autophagosome. The complete characterization of the replicative ACV will be the subject of future studies.

Several MDR *A. baumannii* strains carry LCPs. These plasmids control the expression of diverse chromosomally-encoded genes. Specifically, pAB5, the LCP of UPAB1, differentially regulates the expression of various genes, directly impacting host virulence. We found that UPAB1 cured of its plasmid is unable to replicate within macrophages, suggesting that genetic elements upregulated by the plasmid are likely involved in facilitating intracellular replication. We previously reported that pAB5 upregulates putative T1SS effectors[5]. UPAB1 carries two T1SS loci, and our data revealed that mutants in both systems are defective in intracellular replication. Although the T3SS, T4SS, and T6SS are most commonly involved in manipulation of intracellular pathways, the T1SS is involved in invasion and intracellular replication in other bacterial pathogens, such as *Legionella pneumophila*, *Ehrlichia chaffeensis*, *Francisella novicida* and *Orientia tsutsugamushi*[27–30]. Our proteomic analysis identified several proteins whose secretion is significantly reduced in the individual T1SS mutants. However, since deletion of the T1SS in *A. nosocomialis* resulted in the downregulation of other secretion systems[31], the assignment of these proteins as T1SS effectors awaits further validation. Nevertheless, these experiments uncover several interesting, secreted proteins that may play a role in intracellular replication of UPAB1. Future work will focus on investigating these putative effectors and their possible role in the intracellular lifestyle of *A. baumannii*.

bioRxiv preprint doi: https://doi.org/10.1101/2021.04.08.439081; this version posted April 9, 2021. The copyright holder for this preprint (which was not certified by peer review) is the author/funder, who has granted bioRxiv a license to display the preprint in perpetuity. It is made available under aCC-BY-NC-ND 4.0 International license.

Depletion of macrophages enhances sepsis and severity of disease, demonstrating that macrophages play an important role in eradicating *A. baumannii* infection[11]. Therefore, survival and replication of *A. baumannii* in this type of cells may be a previously underappreciated and important feature of this bacterium. We have also shown that UPAB1 can escape the macrophages by a lytic mechanism. *A. baumannii* could subsequently be phagocytosed by other macrophages and re-start the infection process. Thus, we propose that by replicating inside vacuoles in macrophages, *A. baumannii* evades the immune response and disseminates, resulting in hypervirulent phenotypes. Furthermore, it is tempting to speculate that antibiotics cannot reach the lumen of the ACV, which may contribute to tolerance of *A. baumannii* to antibiotics. Identifying the bacterial factors involved in the intracellular cycle of MDR *A. baumannii* may enable the design of new therapies to combat this pathogen.

Materials and methods

Bacterial strains and culture conditions

The bacterial strains used in this study are listed in Table S1. Unless otherwise noted, strains were grown in lysogeny broth (LB) liquid medium under shaking conditions (200 rpm), or in LB-agar at 37°C. When required, antibiotics were used at the following concentrations: zeocin 50 µg/ml, kanamycin 30 µg/ml, gentamicin 15 µg/ml, and chloramphenicol 15 µg/ml.

DNA manipulations

DNA manipulations were performed according to standard techniques. PCR reactions were performed using Phusion High Fidelity DNA polymerase (New England Biolabs), according to the manufacturer's instructions. Genetic manipulations were carried out in *Escherichia coli* Stellar™ competent cells (Clontech). Primers and plasmids used in this study are listed in Table S2 and S3, respectively.

The *gfp* gene was PCR amplified from pBAV1K-t5-gfp[32] and cloned into pUC18T-mini-Tn*7*T-Zeo by In-Fusion® Cloning (Takara). The pUC18T-mini-Tn*7*T-Zeo-GFP vector was conjugated to *Acinetobacter* as described[33]. All transconjugant strains were confirmed by PCR analysis and fluorescence microscopy.

Construction of *A. baumannii* mutant strains

Mutants were constructed as described previously[34]. Briefly, a FRT site-flanked zeocin resistance cassette was amplified from a variant of pKD4[35] with primers harboring 18–25 nucleotides of homology to the flanking regions of the targeted gene to delete. Upstream and

bioRxiv preprint doi: https://doi.org/10.1101/2021.04.08.439081; this version posted April 9, 2021. The copyright holder for this preprint (which was not certified by peer review) is the author/funder, who has granted bioRxiv a license to display the preprint in perpetuity. It is made available under aCC-BY-NC-ND 4.0 International license.

downstream flanking regions were also amplified, and fragments were assembled by overlap extension PCR. This PCR product was electroporated into competent UPAB1 carrying pAT04, which expresses the RecAB recombinase[34]. Mutants were selected for with zeocin treatment, and integration of the resistance marker was confirmed by PCR. To remove the zeocin resistance cassette, electrocompetent mutants were transformed with pAT03 plasmid, which expresses the FLP recombinase. Zeocin-sensitive clones of clean deletion mutants were obtained. All mutant strains were confirmed by antibiotic resistance profile, PCR, and sequencing.

Cell culture conditions

J774A.1 (ATCC® TIB-67™) mouse macrophage cell line was cultured in Dulbecco's Modified Eagle Medium (DMEM) High Glucose (Hyclone, SH30022.01) supplemented with 10% inactivated Fetal Bovine Serum (FBS, Corning) at 37°C and 5% CO_2. THP-1 (ATCC® TIB-202™) human monocyte cell line was cultured in RPMI-1640 medium (Sigma, R8758) supplemented with 10% FBS, 0.01% MEM Non-Essential Amino Acids (Corning, 25-025-Cl), and 50 µM 2-mercaptoethanol at 37°C and 5% CO_2. For the infection experiments, the THP-1 monocytes were differentiated to macrophages by supplementing the medium with 40 ng/ml of phorbol 12-myristate 13-acetate (PMA, AdipoGen Life Sciences) 48 h prior to the infection.

The bone marrow derived macrophages (BMDM) were obtained from wild-type BALB/c mice as described previously[36] and cultured in DMEM supplemented with 10% FBS at 37°C and 5% CO_2. For the infection experiments, the BMDM were incubated with 10 ng/ml γ-INF overnight prior to the infection.

Antibiotic protection assay

For the intracellular replication assays, J774A.1 cells were cultured in 48 well plates 12-16 h before the experiment ($3x10^5$ cells/well). *A. baumannii* strains were grown overnight in LB at 37°C under shaking conditions. Bacterial cultures were normalized to OD_{600}=1, washed once with PBS, and an appropriate volume was added to each well to reach an MOI of 10. Plates were centrifuged 10 min at 200 x g and incubated for 1 h at 37°C and 5% CO_2. Cells were washed three times with PBS and subsequently incubated with medium supplemented with 100 µg/ml gentamicin and 400 µg/ml kanamycin to kill extracellular bacteria. At 2 h post infection (p.i.) the concentration of antibiotics was decreased to 30 µg/ml gentamicin and 200 µg/ml kanamycin. At 2, 4, 6, and 8 h p.i., cells were washed and lysed with 0.1% Triton X-100. Colony forming units (CFUs) were determined by serial dilution.

bioRxiv preprint doi: https://doi.org/10.1101/2021.04.08.439081; this version posted April 9, 2021. The copyright holder for this preprint (which was not certified by peer review) is the author/funder, who has granted bioRxiv a license to display the preprint in perpetuity. It is made available under aCC-BY-NC-ND 4.0 International license.

To determine the number of bacteria that egress from the infected cells, the antibiotic containing medium was replaced with antibiotic-free medium. At the indicated time points and after 20 min incubation, the supernatant was recovered and serially diluted to determine CFU. The ratio of released bacteria in relation to the numbers of intracellular bacteria corresponding to each time was then calculated.

Immunofluorescence staining

For LC3B staining, samples were fixed with ice cold 100% methanol for 5 min at room temperature, permeabilized with 1% saponin for 20 min, and blocked with 1% PBS-BSA for 1 h. The glass cover slips were incubated with the primary antibody rabbit anti-LC3 (Sigma) at a 1:100 dilution for 3 h at room temperature, then washed 3 times with 1X PBS and incubated with the secondary antibody goat anti-rabbit Alexa 594 (Invitrogen) at a 1:100 dilution and DAPI for 1 h at room temperature. Afterwards, samples were washed with PBS and mounted with ProLong Glass Antifade Mountant solution (Invitrogen).

Confocal microscopy

Infected cells were analyzed with a Zeiss LSM880 laser scanning confocal microscope (Carl Zeiss Inc.) equipped with 405nm diode, 488nm Argon, 543nm HeNe, and 633nm HeNe lasers. A Plan-Apochromat 63X (NA 1.4) DIC objective and ZEN black 2.1 SP3 software were used for image acquisition.

Live imaging

$8x10^5$ J774A.1 cells were plated in a 10 mm Glass Bottom Culture 35 mm petridish (MATEK corporation, P35G-0-14-C) 12-16 h prior to the infection. On the following day, a gentamicin-kanamycin protection assay was performed using UPAB1 GFP at an MOI=10 as described above. At 2 h p.i., cells were incubated in DMEM without phenol red (Hyclone) supplemented with 10% FBS, 30 µg/ml gentamicin, and 200 µg/ml kanamycin. Imaging started at 3.5 h p.i. and pictures were taken every 10 or 20 min.

Time lapse microscopy

Live images were acquired on a Zeiss Observer Z1 inverted microscope equipped with a temperature-controlled CO_2 incubation chamber. Fluorescence images were acquired with illumination from a Colibri 7 LED light source (Zeiss) and ORCA-ER digital camera (Hammamatsu Photonics, Japan). A Plan-Apochromat 63X (NA 1.4) Phase 3 objective and ZEN blue 2.5 software were used for image acquisition.

bioRxiv preprint doi: https://doi.org/10.1101/2021.04.08.439081; this version posted April 9, 2021. The copyright holder for this preprint (which was not certified by peer review) is the author/funder, who has granted bioRxiv a license to display the preprint in perpetuity. It is made available under aCC-BY-NC-ND 4.0 International license.

Transmission electron microscopy

For the Transmission Electron Microscopy (TEM) assay, J774A.1 cells were cultured in 24 well plates 12-16 h before the experiment ($2.5x10^5$ cells/well). The next day, an antibiotic protection assay was performed using UPAB1 GFP at an MOI=10. At 4, 5, and 7 h p.i., the cells were washed, detached with a scraper, and pooled together. Cells were fixed in 2% paraformaldehyde/2.5% glutaraldehyde (Polysciences Inc., Warrington, PA) in 100 mM sodium cacodylate buffer pH 7.2 for 1 h at room temperature and subsequently transferred to 4°C overnight. Samples were washed in sodium cacodylate buffer at room temperature and postfixed in 1% osmium tetroxide (Polysciences Inc.) for 1 h. Samples were then rinsed extensively in distilled water prior to bloc staining with 1% aqueous uranyl acetate (Ted Pella Inc., Redding, CA) for 1 h. Following several rinses in distilled water, samples were dehydrated in a graded series of ethanol and embedded in Eponate 12 resin (Ted Pella Inc.). Sections of 95 nm were cut with a Leica Ultracut UCT ultramicrotome (Leica Microsystems Inc., Bannockburn, IL), stained with uranyl acetate and lead citrate, and viewed on a JEOL 1200 EX transmission electron microscope (JEOL USA Inc., Peabody, MA) equipped with an AMT 8 megapixel digital camera and AMT Image Capture Engine V602 software (Advanced Microscopy Techniques, Woburn, MA).

Cytotoxicity assay

Lactate dehydrogenase (LDH) activity was measure with the CytoTox-One™ Homogeneous Membrane Integrity Assay kit (Promega), according to the manufacturer directions. Enzymatic activity, as a signal of damage of plasma membrane, was measured from the supernatants of infected cells at 24 h p.i. Non-infected cells were included as a negative control, and cells treated with 0.1% Triton X-100 were the 100% lysis control.

Secreted protein enrichment for quantitative proteomics analysis

UPAB1 and derivative strains were grown overnight in 5 ml of M9 minimal medium supplemented with 0.2% casamino acids (M9CAA) and subsequently diluted to OD_{600}=0.05 in 100 ml of fresh M9CAA. Cultures were incubated to mid-log phase and centrifuged at 15,000 x g for 2 min. Supernatants were filter-sterilized with Steriflip vacuum-driven filtration devices (Millipore), concentrated with an Amicon Ultra (Millipore) concentrator with a 10-kDa molecular weight cutoff, flash frozen, and lyophilized. Lyophilized samples were then processed for mass spectrometry analysis as described below. Four individual 100-ml culture biological replicates were prepared for each strain.

bioRxiv preprint doi: https://doi.org/10.1101/2021.04.08.439081; this version posted April 9, 2021. The copyright holder for this preprint (which was not certified by peer review) is the author/funder, who has granted bioRxiv a license to display the preprint in perpetuity. It is made available under aCC-BY-NC-ND 4.0 International license.

Digestion of secretome samples

Precipitated secretomes were resuspended in 6 M urea and 2 M thiourea with 40 mM NH_4HCO_3 and then reduced for 1 h with 20 mM DTT. Reduced samples were then alkylated with 50 mM iodoacetamide for 1 h in the dark. The alkylation reaction was then quenched by the addition of 50 mM DTT for 15 min, and samples were digested with Lys-C (1/200 w/w) for 3 h at room temperature. Samples were diluted with 100 mM NH_4HCO_3 four-fold to reduce the urea/thiourea concentration below 2M, and then an overnight trypsin (1/50 w/w) digestion was performed at room temperature. Digested samples were acidified to a final concentration of 0.5% formic acid and desalted with home-made high-capacity StageTips composed of 1 mg Empore™ C18 material (3M) and 5 mg of OLIGO R3 reverse phase resin (Thermo Fisher Scientific) as previously described [37,38]. Columns were wet with Buffer B (0.1% formic acid, 80% acetonitrile) and conditioned with Buffer A* (0.1% TFA, 2% acetonitrile) prior to use. Acidified samples were loaded onto conditioned columns, washed with 10 bed volumes of Buffer A*, and bound peptides were eluted with Buffer B before being dried then stored at -20˚C.

LC-MS analysis of secretome samples

Dried secretome digests were re-suspended in Buffer A* and separated using a two-column chromatography set up composed of a PepMap100 C18 20 mm x 75 µm trap and a PepMap C18 500 mm x 75 µm analytical column (Thermo Fisher Scientific). Samples were concentrated onto the trap column at 5 µl/min for 5 min with Buffer A (0.1% formic acid, 2% DMSO) and then infused into an Orbitrap Q-Exactive plus Mass Spectrometer (Thermo Fisher Scientific) at 300 nl/min via the analytical column using a Dionex Ultimate 3000 UPLC (Thermo Fisher Scientific). 125-min analytical runs were undertaken by altering the buffer composition from 2% (0.1% formic acid, 77.9% acetonitrile, 2% DMSO) to 22% Buffer B over 95 min, then from 22% to 40% Buffer B over 10 min, and 40% to 80% Buffer B over 5 min. The composition was held at 80% Buffer B for 5 min and then dropped to 2% over 2 min before being held at 2% for another 8 min. The Q-Exactive plus Mass Spectrometer was operated in a data-dependent mode automatically switching between the acquisition of a single Orbitrap MS scan (375-1400 m/z, maximal injection time of 50 ms, an Automated Gain Control (AGC) set to a maximum of $3*10^6$ ions, and a resolution of 70k) and up to 15 Orbitrap MS/MS HCD scans of precursors (Stepped NCE of 28%, 30% and 35%, a maximal injection time of 100 ms, an AGC set to a maximum of $2*10^5$ ions, and a resolution of 17.5k).

Proteomic analysis

bioRxiv preprint doi: https://doi.org/10.1101/2021.04.08.439081; this version posted April 9, 2021. The copyright holder for this preprint (which was not certified by peer review) is the author/funder, who has granted bioRxiv a license to display the preprint in perpetuity. It is made available under aCC-BY-NC-ND 4.0 International license.

Secretome samples were processed using MaxQuant (v1.6.17.0.[39]) and searched against the NCBI annotated *A. baumannii* UPAB1 proteome (NCBI Accession: PRJNA487603, 3750 proteins, downloaded 2020-3-10), a six-frame translation of the UPAB1 genome generated using the six-frame translation generator within Maxquant, and the ATCC17978 proteome (Uniprot: UP000319385, 3627 proteins, downloaded 2014-11-16) to allow the use of Uniprot annotation information associated with ATCC17978 proteins. Searches were undertaken using "Trypsin" enzyme specificity with carbamidomethylation of cysteine as a fixed modification. Oxidation of methionine and acetylation of protein N-termini were included as variable modifications, and a maximum of 2 missed cleavages were allowed. To enhance the identification of peptides between samples, the Match between Runs option was enabled with a precursor match window set to 2 min and an alignment window of 20 min with the label free quantitation (LFQ) option enabled[40]. The resulting outputs were processed within the Perseus (v1.6.0.7) analysis environment[41] to remove reverse matches and common protein contaminates prior to further analysis. For LFQ comparisons, biological replicates were grouped and data was filtered to remove any protein which was not observed in at least one group three times. Missing values were then imputed based on the observed total peptide intensities with a range of 0.3σ and a downshift of 2.5σ using Perseus. Student *t* tests were undertaken to compare the secretome between groups with the resulting data exported and visualized using ggplot2[42] within R. The resulting MS data and search results have been deposited into the PRIDE ProteomeXchange Consortium repository[43,44] and can be accessed with the identifier:PXD024736 using the Username: reviewer_pxd024736@ebi.ac.uk and Password: YS5qjHcG.

Statistical analysis

All statistical analyses were performed using GraphPad Prism 8.0 (GraphPad Software Inc., La Jolla, CA). For all datasets, Student's unpaired *t*-tests were used.

Data availability

The authors declare that data supporting the findings of this study are available within the paper and its supplemental files. The resulting MS data and search results have been deposited into the PRIDE ProteomeXchange Consortium repository[43,44] and can be accessed with the identifier PXD024736 using the Username: reviewer_pxd024736@ebi.ac.uk and Password: YS5qjHcG.

Table S1. Bacterial strains.

bioRxiv preprint doi: https://doi.org/10.1101/2021.04.08.439081; this version posted April 9, 2021. The copyright holder for this preprint (which was not certified by peer review) is the author/funder, who has granted bioRxiv a license to display the preprint in perpetuity. It is made available under aCC-BY-NC-ND 4.0 International license.

Bacterial strain	**Description**	**Reference**
Acinetobacter baumannii		
UPAB1	MDR urine isolate with pAB5 plasmid	[20]
UPAB1p-	Derivative strain without pAB5	[20]
19606	Urinary tract infection isolate	[45]
286	*A.b.* HUC88.01. Urinary tract infection clinical isolate	This work.
398	*A.b.* 1955182	IHMA Labs.
413	Clinical isolate. ACATPM 4061-2	U. of Pittsburgh.
414	Clinical isolate. ACATPM 4079	U. of Pittsburgh.
UPAB1 GFP	GFP-expressing transconjugant	This work.
19606 GFP	GFP-expressing transconjugant	This work.
286 GFP	GFP-expressing transconjugant	This work.
398 GFP	GFP-expressing transconjugant	This work.
ΔhlyB1	UPAB1 strain with an unmarked deletion of the *hlyB1* (D1G37_13690) gene corresponding to the T1SSa	This work.
ΔhlyD2	UPAB1 strain with an unmarked deletion of the *hlyD2* (DG137_00070) gene corresponding to the T1SSb	This work.
ΔhlyB1,ΔhlyD2	UPAB1 strain with an unmarked deletion of the *hlyB1* (D1G37_13690) and *hlyD2* (DG137_00070) genes	This work.
Serratia marcescens		
Serratia marcescens GFP	RM 66262 expressing GFP.	[15]
Escherichia coli		
Stellar™ Competent Cells	*F–, endA1, supE44, thi-1, recA1, relA1, gyrA96, phoA, Φ80d lacZΔ M15, Δ(lacZYA-argF) U169, Δ(mrr-hsdRMS-mcrBC), ΔmcrA, λ–*	Clontech.

420 **Table S2. List of primers used in this study.**

Primers	
UpstB1F	GCGAGTCAAGCAGACCCAATTC
UpstB1R	CAGCTCCAGCCTACACAATCGCTGGTTGTACTTCGAACCCCTGAAT
DownstB1F	GAACTAAGGAGGATATTCATATGATGAGCGAACAACAACAAGAATTTACC
DownstB1R	TCTTTTACGACACCGCGCAC
UpstD1F	CTTGCGATCCGCCATTTAAAAATTCG
UpstD1R	CAGCTCCAGCCTACACAATCGCTGAATTGCCCCCTTGGCTCAC
DownstD1F	GGAATAGGAACTAAGGAGGATATTCATATGGAAAAAAAGCCCCGAAA
DownstD1R	CTTCGCGACCACGAGTCAC
UpstB2F	TAAATCGGTCGCCTGACGTTTC
UpstB2R	CAGCTCCAGCCTACACAATCGCTATGAGTTATAAACAGCTGAATTGGGCT
DownstB2	GAACTAAGGAGGATATTCATATGGGCTCAATTTTGAATCCTTGAATAGAAGTA

bioRxiv preprint doi: https://doi.org/10.1101/2021.04.08.439081; this version posted April 9, 2021. The copyright holder for this preprint (which was not certified by peer review) is the author/funder, who has granted bioRxiv a license to display the preprint in perpetuity. It is made available under aCC-BY-NC-ND 4.0 International license.

F	TCA
DownstB2 R	AGCCGATCCAGTACAAGCTCAG
UpstD2F	CGTCAACAAGGTCGGCCTAATT
UpstD2R	AGCTCCAGCCTACACAATCGCTTAAATCTTCAAAAAATAAGAATTTTACAGTGG ATTTAT
DownstD2 F	GAACTAAGGAGGATATTCATATGCATTCGGCTCCTATTTTTTGCTTTGG
DownstD2 R	CAACCTCCTCGTGCACATCTC
P1	AGCGATTGTGTAGGCTGGAGCTG
P2	CATATGAATATCCTCCTTAGTTCCTATTCC
GFP Fw	TGAGCTCACTAGTGGATCCCCAATTCACTGTTCCTTGC
GFP Rv	GGCATGGATGAACTATACAAATAAAAGCTTGGGCCCGGTACC
pUCT-lin-Fw	AAGCTTGGGCCCGGTACC
pUCT-lin-Rv	GCATGAGCTCACTAGTGGATCC

Table S3. List of plasmids used in this study.

Plasmid	Description
pBAV1k-t5-gfp	published vector [32], kanamycin resistance marker
pUC18T-mini-Tn*7*T-Zeo	published vector [33], zeocin resistance marker
pUC18T-mini-Tn*7*T-Zeo-GFP	promotor promlac and *gfp* gene from pBAV1k-t5-gfp on pUC18T-mini-Tn*7*T-Zeo backbone, zeocin resistance marker

Acknowledgments

We thank the imaging laboratory of the Molecular Microbiology Department at Washington University in St Louis. We thank Dr. Rachel L. Kinsella for kindly providing BMDM. We thank the members of the Feldman lab for critical reading of the manuscript. This work was supported by grants from the National Institute of Allergy and Infectious Diseases (grants R01AI144120).

Author Contributions

Conceived and designed the experiments: GS GD MGS MFF. Performed the experiments: GS GD MGS NHL NES WLB. Analyzed the data: GS GD MGS NES MFF. Wrote the paper: GD MFF.

Conflict of Interest

All authors report no conflict of interests.

bioRxiv preprint doi: https://doi.org/10.1101/2021.04.08.439081; this version posted April 9, 2021. The copyright holder for this preprint (which was not certified by peer review) is the author/funder, who has granted bioRxiv a license to display the preprint in perpetuity. It is made available under aCC-BY-NC-ND 4.0 International license.

Bibliography

1. Weiner LM, Webb AK, Limbago B, Dudeck MA, Patel J, Kallen AJ, et al. Antimicrobial-Resistant Pathogens Associated With Healthcare-Associated Infections: Summary of Data Reported to the National Healthcare Safety Network at the Centers for Disease Control and Prevention, 2011–2014. Infect Control Hosp Epidemiol. 2016;37: 1288–1301. doi:10.1017/ice.2016.174

2. Valencia R, Arroyo LA, Conde M, Aldana JM, Torres M-J, Fernández-Cuenca F, et al. Nosocomial outbreak of infection with pan-drug-resistant Acinetobacter baumannii in a tertiary care university hospital. Infect Control Hosp Epidemiol. 2009;30: 257–63. doi:10.1086/595977

3. Tacconelli E, Magrini N, Kahlmeter G, Singh N. Global Priority List of Antibiotic-Resistant Bacteria To Guide Research, Discovery, and Development of New Antibiotics. 2017.

4. Centers for Disease Control U. Antibiotic Resistance Threats in the United States, 2019. [cited 8 Apr 2021]. doi:10.15620/cdc:82532

5. Di Venanzio G, Flores-Mireles AL, Calix JJ, Haurat MF, Scott NE, Palmer LD, et al. Urinary tract colonization is enhanced by a plasmid that regulates uropathogenic Acinetobacter baumannii chromosomal genes. Nat Commun. 2019;10: 1–13. doi:10.1038/s41467-019-10706-y

6. Kinsella RL, Lopez J, Palmer LD, Salinas ND, Skaar EP, Tolia NH, et al. Defining the interaction of the protease CpaA with its type II secretion-chaperone CpaB and its contribution to virulence in Acinetobacter species. 2017. doi:10.1074/jbc.M117.808394

7. An Z, Huang X, Zheng C, Ding W. Acinetobacter baumannii outer membrane protein A induces HeLa cell autophagy via MAPK/JNK signaling pathway. Int J Med Microbiol. 2018 [cited 15 Jan 2019]. doi:10.1016/J.IJMM.2018.12.004

8. Wang Y, Zhang K, Shi X, Wang C, Wang F, Fan J, et al. Critical role of bacterial isochorismatase in the autophagic process induced by Acinetobacter baumannii in mammalian cells. FASEB J. 2016; 1–15. doi:10.1096/fj.201500019R

9. Bist P, Dikshit N, Koh TH, Mortellaro A, Tan TT, Sukumaran B. The Nod1, Nod2, and Rip2 Axis Contributes to Host Immune Defense against Intracellular Acinetobacter baumannii Infection. Infect Immun. 2014;82: 1112–1122. doi:10.1128/IAI.01459-13

10. Parra-Millán R, Guerrero-Gómez D, Ayerbe-Algaba R, Pachón-Ibáñez ME, Miranda-Vizuete A, Pachón J, et al. Intracellular Trafficking and Persistence of *Acinetobacter baumannii* Requires Transcription Factor EB. mSphere. 2018;3: e00106-18. doi:10.1128/mSphere.00106-18

11. Grguric-Smith LM, Lee HH, Gandhi JA, Brennan MB, DeLeon-Rodriguez CM, Coelho C, et al. Neutropenia exacerbates infection by Acinetobacter baumannii clinical isolates in a murine wound model. Front Microbiol. 2015;6: 1134. doi:10.3389/fmicb.2015.01134

12. Rumbo C, Tomás M, Moreira EF, Soares NC, Carvajal M, Santillana E, et al. The Acinetobacter baumannii Omp33-36 porin is a virulence factor that induces apoptosis and modulates autophagy in human cells. Infect Immun. 2014;82: 4666–4680.

bioRxiv preprint doi: https://doi.org/10.1101/2021.04.08.439081; this version posted April 9, 2021. The copyright holder for this preprint (which was not certified by peer review) is the author/funder, who has granted bioRxiv a license to display the preprint in perpetuity. It is made available under aCC-BY-NC-ND 4.0 International license.

478 doi:10.1128/IAI.02034-14

479 13. Jacobs AC, Thompson MG, Black CC, Kessler JL, Clark LP, McQueary CN, et al.
480 AB5075 , a Highly Virulent Isolate of Acinetobacter baumannii , as a Model Strain for the
481 Evaluation of Pathogenesis and Antimicrobial Treatments. MBio. 2014;5: 1–10.
482 doi:10.1128/mBio.01076-14.Editor

483 14. Nakagawa I, Amano A, Mizushima N, Yamamoto A, Yamaguchi H, Kamimoto T, et al.
484 Autophagy defends cells against invading group A Streptococcus. Science (80-).
485 2004;306: 1037–1040. doi:10.1126/science.1103966

486 15. Fedrigo GVGV, Campoy EMEM, Di Venanzio G, Colombo MIMI, García Véscovi E,
487 Véscovi EG. Serratia marcescens Is Able to Survive and Proliferate in Autophagic-Like
488 Vacuoles inside Non-Phagocytic Cells. May RC, editor. PLoS One. 2011;6: 15.
489 doi:10.1371/journal.pone.0024054

490 16. Romano PS, Gutierrez MG, Berón W, Rabinovitch M, Colombo MI. The autophagic
491 pathway is actively modulated by phase II Coxiella burnetii to efficiently replicate in the
492 host cell. Cell Microbiol. 2007;9: 891–909. doi:10.1111/j.1462-5822.2006.00838.x

493 17. Kabeya Y, Mizushima N, Ueno T, Yamamoto A, Kirisako T, Noda T, et al. LC3, a
494 mammalian homologue of yeast Apg8p, is localized in autophagosome membranes after
495 processing. EMBO J. 2000;19: 5720–8. doi:10.1093/emboj/19.21.5720

496 18. Kumar P, Nagarajan A, Uchil PD. Analysis of cell viability by the lactate dehydrogenase
497 assay. Cold Spring Harb Protoc. 2018;2018: 465–468. doi:10.1101/pdb.prot095497

498 19. Venanzio G Di, Moon KH, Weber BS, Lopez J, Ly PM, Potter RF, et al. Multi-drug
499 resistant plasmids repress T6SS to enable their dissemination. Proc Natl Acad Sci U S A.
500 2019;116: 1–23. doi:10.1073/pnas.1812557116

501 20. Di Venanzio G, Flores-Mireles AL, Calix JJ, Haurat MF, Scott NE, Palmer LD, et al.
502 Urinary tract colonization is enhanced by a plasmid that regulates uropathogenic
503 Acinetobacter baumannii chromosomal genes. Nat Commun. 2019;10.
504 doi:10.1038/s41467-019-10706-y

505 21. Weber BS, Ly PM, Irwin JN, Pukatzki S, Feldman MF. A multidrug resistance plasmid
506 contains the molecular switch for type VI secretion in Acinetobacter baumannii. Proc Natl
507 Acad Sci U S A. 2015;112: 9442–7. doi:10.1073/pnas.1502966112

508 22. Costa TRD, Felisberto-Rodrigues C, Meir A, Prevost MS, Redzej A, Trokter M, et al.
509 Secretion systems in Gram-negative bacteria: structural and mechanistic insights. Nat
510 Rev Microbiol. 2015;13: 343–359. doi:10.1038/nrmicro3456

511 23. Harding CM, Hennon SW, Feldman MF. Uncovering the mechanisms of Acinetobacter
512 baumannii virulence. Nat Rev Microbiol. 2017;16: 91–102. doi:10.1038/nrmicro.2017.148

513 24. Lopez J, Ly PM, Feldman MF. The tip of the VgrG spike is essential to functional type VI
514 secretion system assembly in acinetobacter baumannii. MBio. 2020;11: 1–14.
515 doi:10.1128/mBio.02761-19

516 25. Thomas S, Holland IB, Schmitt L. The Type 1 secretion pathway - The hemolysin system
517 and beyond. Biochimica et Biophysica Acta - Molecular Cell Research. Elsevier; 2014.
518 pp. 1629–1641. doi:10.1016/j.bbamcr.2013.09.017

519 26. Teymournejad O, Rikihisa Y. Ehrlichia chaffeensis uses an invasin to suppress reactive

bioRxiv preprint doi: https://doi.org/10.1101/2021.04.08.439081; this version posted April 9, 2021. The copyright holder for this preprint (which was not certified by peer review) is the author/funder, who has granted bioRxiv a license to display the preprint in perpetuity. It is made available under aCC-BY-NC-ND 4.0 International license.

oxygen species generation by macrophages via cd147-dependent inhibition of vav1 to block rac1 activation. MBio. 2020;11. doi:10.1128/mBio.00267-20

27. Saha SS, Uda A, Watanabe K, Shimizu T, Watarai M. RtxA like protein contributes to infection of Francisella novicida in silkworm and human macrophage THP-1. Microb Pathog. 2018;123: 74–81. doi:10.1016/j.micpath.2018.06.046

28. Fuche F, Vianney A, Andrea C, Doublet P, Gilbert C. Functional type 1 secretion system involved in Legionella pneumophila virulence. J Bacteriol. 2015;197: 563–571. doi:10.1128/JB.02164-14

29. Luo T, McBride JW. Ehrlichia chaffeensis TRP32 interacts with host cell targets that influence intracellular survival. Infect Immun. 2012;80: 2297–2306. doi:10.1128/IAI.00154-12

30. VieBrock L, Evans SM, Beyer AR, Larson CL, Beare PA, Ge H, et al. Orientia tsutsugamushi ankyrin repeat-containing protein family members are type 1 secretion system substrates that traffic to the host cell endoplasmic reticulum. Front Cell Infect Microbiol. 2014;4. doi:10.3389/fcimb.2014.00186

31. Harding CM, Pulido MR, Di Venanzio G, Kinsella RL, Webb AI, Scott NE, et al. Pathogenic Acinetobacter species have a functional type i secretion system and contact-dependent inhibition systems. J Biol Chem. 2017;292. doi:10.1074/jbc.M117.781575

32. Bryksin A V., Matsumura I. Rational Design of a Plasmid Origin That Replicates Efficiently in Both Gram-Positive and Gram-Negative Bacteria. Mokrousov I, editor. PLoS One. 2010;5: e13244. doi:10.1371/journal.pone.0013244

33. Ducas-Mowchun K, De Silva PM, Crisostomo L, Fernando DM, Chao TC, Pelka P, et al. Next generation of Tn7-based single-copy insertion elements for use in multi- and pan-drug-resistant strains of Acinetobacter baumannii. Appl Environ Microbiol. 2019;85. doi:10.1128/AEM.00066-19

34. Tucker AT, Nowicki EM, Boll JM, Knauf GA, Burdis NC, Trent MS, et al. Defining gene-phenotype relationships in Acinetobacter baumannii through one-step chromosomal gene inactivation. MBio. 2014;5: e01313–e01314. doi:10.1128/mBio.01313-14

35. Hashim S, Mukherjee K, Raje M, Basu SK, Mukhopadhyay a. Live Salmonella modulate expression of Rab proteins to persist in a specialized compartment and escape transport to lysosomes. J Biol Chem. 2000;275: 16281–8. Available: http://www.ncbi.nlm.nih.gov/pubmed/10821869

36. Kimmey JM, Huynh JP, Weiss LA, Park S, Kambal A, Debnath J, et al. Unique role for ATG5 in neutrophil-mediated immunopathology during M. tuberculosis infection. Nature. 2015;528: 565–569. doi:10.1038/nature16451

37. Ishihama Y, Rappsilber J, Mann M. Modular stop and go extraction tips with stacked disks for parallel and multidimensional Peptide fractionation in proteomics. J Proteome Res. 2006;5: 988–94. doi:10.1021/pr050385q

38. Rappsilber J, Mann M, Ishihama Y. Protocol for micro-purification, enrichment, pre-fractionation and storage of peptides for proteomics using StageTips. Nat Protoc. 2007;2: 1896–906. doi:10.1038/nprot.2007.261

39. Cox J, Mann M. MaxQuant enables high peptide identification rates, individualized p.p.b.-range mass accuracies and proteome-wide protein quantification. Nat Biotechnol.

bioRxiv preprint doi: https://doi.org/10.1101/2021.04.08.439081; this version posted April 9, 2021. The copyright holder for this preprint (which was not certified by peer review) is the author/funder, who has granted bioRxiv a license to display the preprint in perpetuity. It is made available under aCC-BY-NC-ND 4.0 International license.

2008;26: 1367–1372. doi:10.1038/nbt.1511

40. Cox J, Hein MY, Luber CA, Paron I, Nagaraj N, Mann M. Accurate proteome-wide label-free quantification by delayed normalization and maximal peptide ratio extraction, termed MaxLFQ. Mol Cell Proteomics. 2014;13: 2513–26. doi:10.1074/mcp.M113.031591

41. Tyanova S, Temu T, Sinitcyn P, Carlson A, Hein MY, Geiger T, et al. The Perseus computational platform for comprehensive analysis of (prote)omics data. Nat Methods. 2016;13: 731–40. doi:10.1038/nmeth.3901

42. Wickham H. ggplot2 - Elegant Graphics for Data Analysis | . New York: Springer-Verlag; 2016. Available: https://www.springer.com/gp/book/9783319242750

43. Vizcaíno JA, Csordas A, del-Toro N, Dianes JA, Griss J, Lavidas I, et al. 2016 update of the PRIDE database and its related tools. Nucleic Acids Res. 2016;44: D447–D456. doi:10.1093/nar/gkv1145

44. Perez-Riverol Y, Csordas A, Bai J, Bernal-Llinares M, Hewapathirana S, Kundu DJ, et al. The PRIDE database and related tools and resources in 2019: Improving support for quantification data. Nucleic Acids Res. 2019;47: D442–D450. doi:10.1093/nar/gky1106

45. Hugh R, Reese R. Designation of the type strain for Bacterium anitratum Schaub and Hauber 1948. Int J Syst Bacteriol. 1967;17: 245–254. doi:10.1099/00207713-17-3-245

bioRxiv preprint doi: https://doi.org/10.1101/2021.04.08.439081; this version posted April 9, 2021. The copyright holder for this preprint (which was not certified by peer review) is the author/funder, who has granted bioRxiv a license to display the preprint in perpetuity. It is made available under aCC-BY-NC-ND 4.0 International license.

Figure Legends

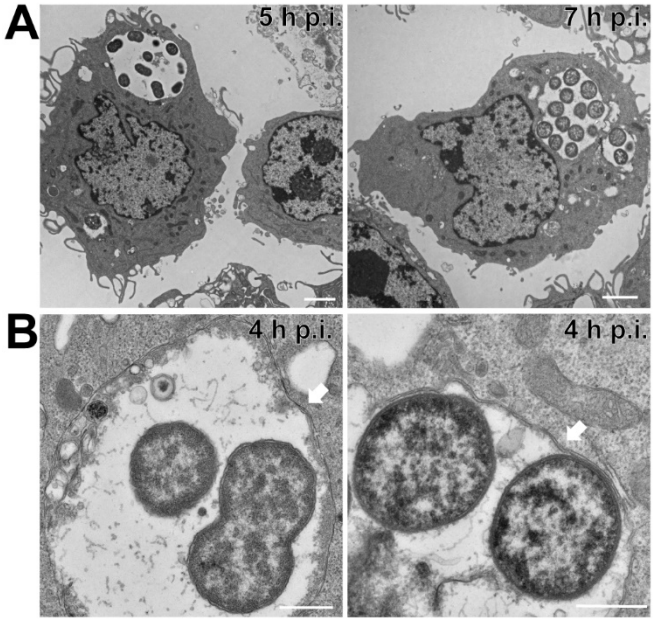

Figure 1. UPAB1 resides in spacious vacuoles within macrophages. Transmission electron microscopic images of J77A.1 macrophages infected with UPAB1 (**A**) at 5 (left panel) and 7 h p.i. (right panel) Bars: 2 µm. (**B**) The UPAB1 containing vacuole can be single (left panel) or double membrane (right panel). Bars: 500 nm.

bioRxiv preprint doi: https://doi.org/10.1101/2021.04.08.439081; this version posted April 9, 2021. The copyright holder for this preprint (which was not certified by peer review) is the author/funder, who has granted bioRxiv a license to display the preprint in perpetuity. It is made available under aCC-BY-NC-ND 4.0 International license.

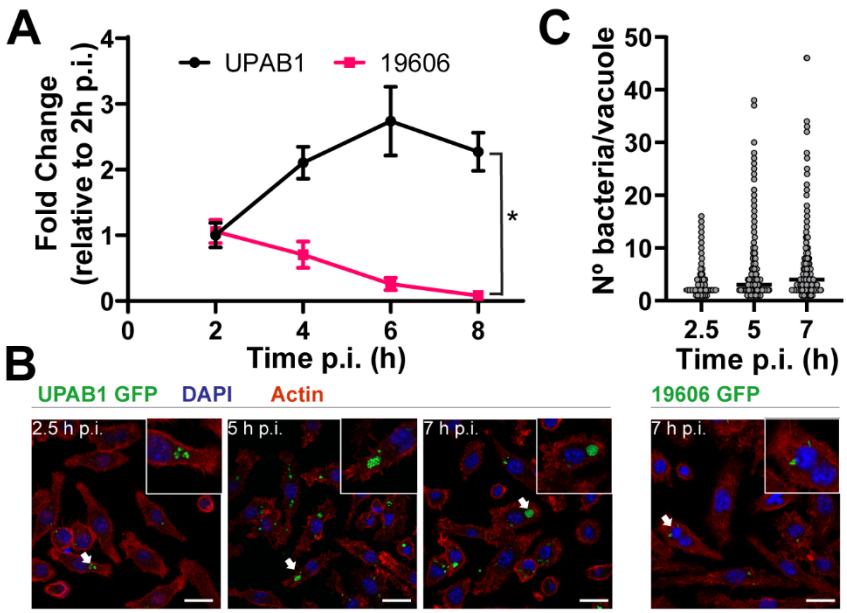

Figure 2. UPAB1 but not 19606 replicate in macrophages. (A) J774A.1 macrophages were infected with the indicated strains, and after phagocytosis, extracellular bacteria was eliminated with antibiotics. After different time points, total numbers of intracellular CFU were determined. *$p < 0.05$. **(B)** Representative images of infected cells at the indicated time points. Samples were stained for cell nuclei (blue), actin (red) and *Acinetobacter* expressed GFP (green). Insets show a higher magnification of the area indicated by the white arrow. Bars: 20 μm **(C)** Quantification of bacteria per vacuole at different times p.i. Each symbol represents an individual vacuole, horizontal line represents the median. At least 200 infected cells were analyzed for each time point for three independent experiments.

bioRxiv preprint doi: https://doi.org/10.1101/2021.04.08.439081; this version posted April 9, 2021. The copyright holder for this preprint (which was not certified by peer review) is the author/funder, who has granted bioRxiv a license to display the preprint in perpetuity. It is made available under aCC-BY-NC-ND 4.0 International license.

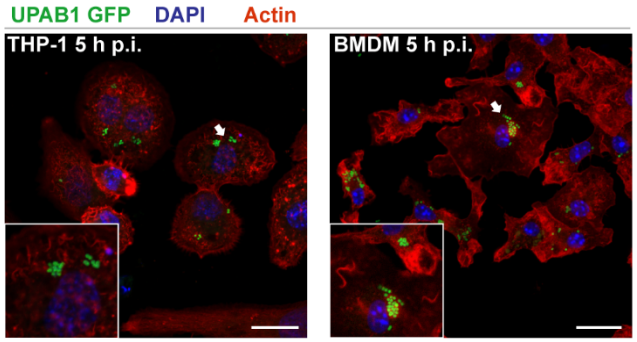

Figure 3. UPAB1 replicates in multiple host cell lines. Representative images of infected THP-1 (left panel) or BMDM (right panel) cells at 5 h p.i. Samples were stained for cell nuclei (blue), actin (red) and *Acinetobacter* expressed GFP (green). Insets show a higher magnification of the area indicated by the white arrow. Bars: 20 µm.

bioRxiv preprint doi: https://doi.org/10.1101/2021.04.08.439081; this version posted April 9, 2021. The copyright holder for this preprint (which was not certified by peer review) is the author/funder, who has granted bioRxiv a license to display the preprint in perpetuity. It is made available under aCC-BY-NC-ND 4.0 International license.

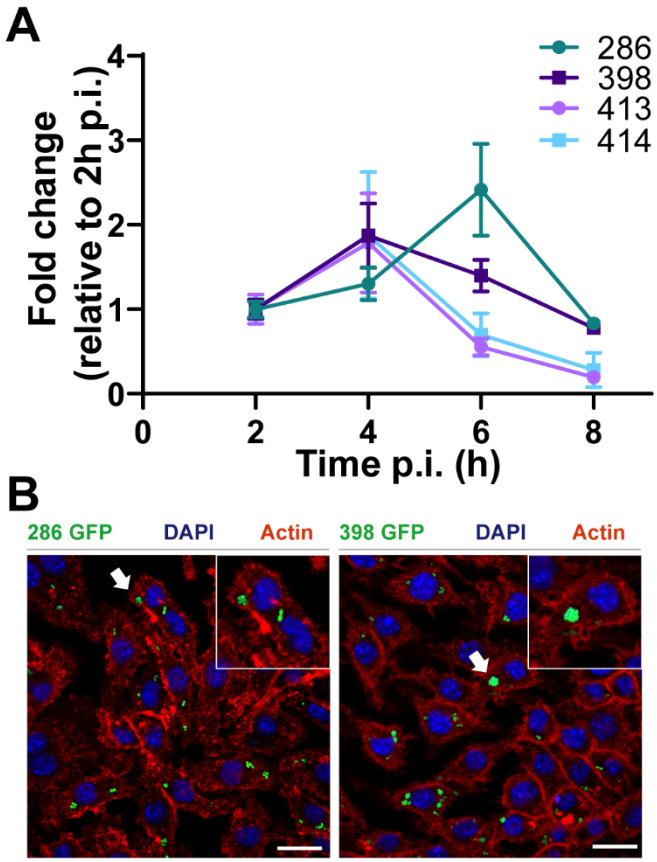

Figure 4. Recent clinical isolates replicate in macrophages. (A) J774A.1 macrophages were infected with the indicated strains, and after phagocytosis, extracellular bacteria was eliminated with antibiotics. After different time points, total numbers of intracellular CFU were determined. Data represent mean and standard deviation values for 3 independent experiments. **(B)** Representative images of infected cells with the indicated strains. Samples were stained for cell nuclei (blue), actin (red) and *Acinetobacter* expressed GFP (green). Insets show a higher magnification of the area indicated by the white arrow. Bars: 20 µm.

bioRxiv preprint doi: https://doi.org/10.1101/2021.04.08.439081; this version posted April 9, 2021. The copyright holder for this preprint (which was not certified by peer review) is the author/funder, who has granted bioRxiv a license to display the preprint in perpetuity. It is made available under aCC-BY-NC-ND 4.0 International license.

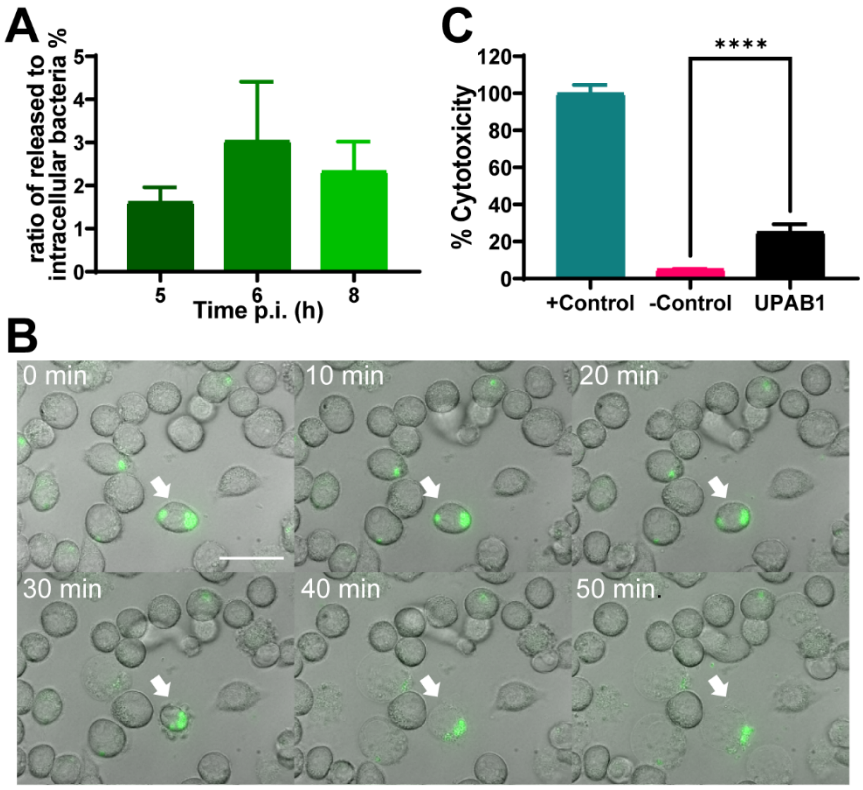

Figure 5. UPAB1 escapes the macrophages by a lytic process. J774A.1 macrophages were infected with UPAB1. **(A)** At different time points, antibiotic containing medium was replaced by antibiotic- free medium. CFU in supernatants were determined and the ratio of released to intracellular bacteria was calculated. Data represent mean and standard deviation values for 3 independent experiments. **(B)** Images from time-lapse microscopy showing UPAB1 egress from the invaded macrophages. J774A.1 cells were invaded with UPAB1 GFP (green fluorescence). At 7 h p.i. images were taken every 10 min and analyzed with ImageJ software. The white arrow indicates the invaded cell. Bars: 20 µm. **(C)** LDH activity in the supernatant of infected macrophages was measured at 24 h p.i. Percentage of cytotoxicity was calculated as the activity of released LDH relative to total LDH activity. The mean ± S.D. for two independent experiments is shown. **** $p < 0.0001$.

bioRxiv preprint doi: https://doi.org/10.1101/2021.04.08.439081; this version posted April 9, 2021. The copyright holder for this preprint (which was not certified by peer review) is the author/funder, who has granted bioRxiv a license to display the preprint in perpetuity. It is made available under aCC-BY-NC-ND 4.0 International license.

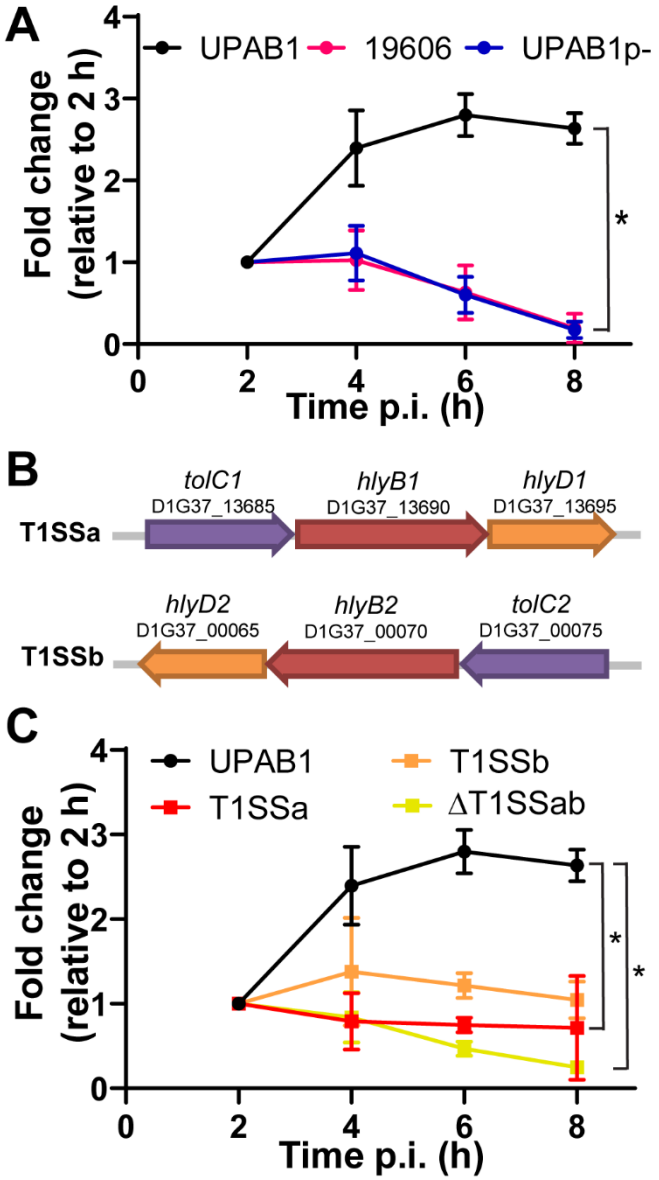

628

629 **Figure 6. pAB5 and T1SS are required for UPAB1 intracellular replication. (A)** J774A.1
630 macrophages were infected with the indicated strains. UPAB1p- strain is not able to replicate.
631 Data represents mean and standard deviation values for 3 independent experiments.
632 *p < 0.05. **(B)** Genetic organization of the T1SSa and T1SSb locus. **(C)** Individual and double
633 T1SS mutants have a defect in intracellular replication in J774A.1 macrophages. Data
634 represents mean and standard deviation values, for 3 independent experiments. *p < 0.05.

635

bioRxiv preprint doi: https://doi.org/10.1101/2021.04.08.439081; this version posted April 9, 2021. The copyright holder for this preprint (which was not certified by peer review) is the author/funder, who has granted bioRxiv a license to display the preprint in perpetuity. It is made available under aCC-BY-NC-ND 4.0 International license.

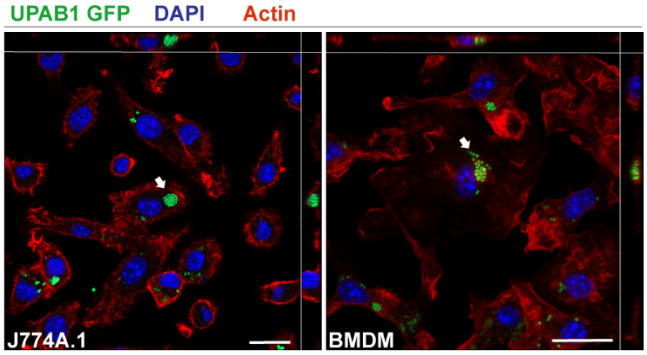

Figure S1. UPAB1 replicates in multiple host cell lines. Representative Z-stacks of infected J774A.1 cells (left panel) or BMDM (right panel) at 7 and 5 h p.i., respectively. Samples were stained for cell nuclei (blue), actin (red) and *Acinetobacter* expressed GFP (green). Insets show a higher magnification of the area indicated by the white arrow. Bars: 20 µm.

bioRxiv preprint doi: https://doi.org/10.1101/2021.04.08.439081; this version posted April 9, 2021. The copyright holder for this preprint (which was not certified by peer review) is the author/funder, who has granted bioRxiv a license to display the preprint in perpetuity. It is made available under aCC-BY-NC-ND 4.0 International license.

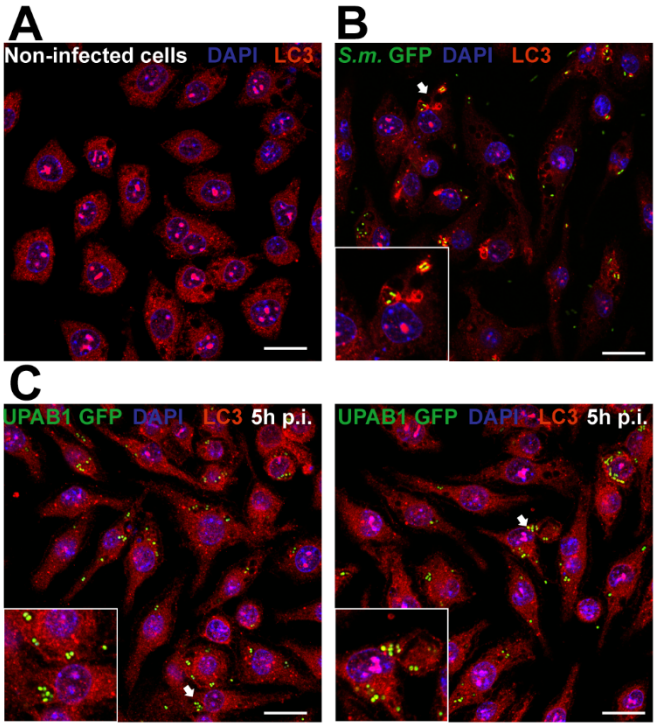

Figure S2. UPAB1 ACV are LC3 negative. Representative images of (A) non-infected, (B) Serratia marcescens-infected, or (C) UPAB1-infected J774A.1 macrophages. Samples were stained for cell nuclei (blue), LC3 (red) and bacteria expressed GFP (green). Insets show a higher magnification of the area indicated by the white arrow. Bars: 20 µm.

bioRxiv preprint doi: https://doi.org/10.1101/2021.04.08.439081; this version posted April 9, 2021. The copyright holder for this preprint (which was not certified by peer review) is the author/funder, who has granted bioRxiv a license to display the preprint in perpetuity. It is made available under aCC-BY-NC-ND 4.0 International license.

Table 1. Putative T1SS-dependent effectors

T-test Difference mut_WT	Locus tag	Predicted function
ΔT1SSa		
-10.5	D1G37_01945	BapA
-9.1	D1G37_04720	OmpA
-5.7	D1G37_05375	PilY1
-5.4	D1G37_18005	Hypothetical protein
-5.2	D1G37_15450	Phosphodiester glycosidase family protein
-5.0	D1G37_13335	Gly zipper domain/ toxic amyloid oligomer
-4.7	D1G37_05180	Secreted serine peptidase
-4.2	D1G37_05495	type IV pilus secretin PilQ
-4.0	D1G37_12590	Curli production component
-3.9	D1G37_01055	Colicin synthesis protein, bactericidal
-3.8	D1G37_10435	Bacteriocin resistance protein, peptidase
-3.8	D1G37_03120	RTX2
-3.8	D1G37_16210	Phosphatase
-3.4	D1G37_05480	Pili operon hypothetical protein
-3.3	D1G37_12980	Hypothetical protein, exported
ΔT1SSb		
-9.9	D1G37_05375	PilY1
-8.0	D1G37_05445	PilA
-3.9	D1G37_04400	invasin/ igG like
-3.7	D1G37_00110	Cell surface protein Ata
-3.6	D1G37_10430	FilA
-3.4	D1G37_11695	Transferrin binding protein
-3.4	D1G37_00700	Hypothetical protein

Cut-off was defined at -3 by a student T-test difference between mutant and WT. Protein localization prediction was performed employing PSORT and presence of signal peptide was analyzed by SignalP.